INVESTIGATION OF LASER PROPAGATION PHONOMENA

Stuart A. Collins, Jr., et al

Ohio State University

Prepared for:

Defense Advanced Research Projects Agency
Rome Air Development Center

December 1973

UNCLASSIFIED

AD775738

DOCUMENT CONTROL DATA R & D

ElectroScience Laboratory,
Department of Electrical Engineering, The Ohio State University, Columbus, Ohio 43212

Unclassified

INVESTIGATION OF LASER PROPAGATION PHENOMENA

4 DESCRIPTIVE NOTES (Type of report and inclusive dates)
Final Technical Report

5 AUTHOR(S) (First name, middle initial, last name)
Collins, S.A., Jr.
Duncan, D.D.

6 REPORT DATE	7a. TOTAL NO. OF PAGES	7b. NO. OF REFS
December 1973	24 30	9

8a CONTRACT OR GRANT NO	9a. ORIGINATOR'S REPORT NUMBER(S)
F30602-72-C-0305	ElectroScience Laboratory 3432-7
b. PROJECT NO	
c.	9b. OTHER REPORT NO(S) (Any other numbers that may be assigned this report)
d.	RADC-TR-74-14

10 DISTRIBUTION STATEMENT
Approved for public release; distribution unlimited

11 SUPPLEMENTARY NOTES	12 SPONSORING MILITARY ACTIVITY
	Defense Advanced Research Projects Agency 1400 Wilson Bldv. Arlington, VA 22209

13 ABSTRACT

This is the final report for the Contract entitled "Investigation of Laser Propagation Phenomena." The object of the contract has been to provide theoretical studies of selected topics associated with light-beam propagation through a turbulent atmosphere for a program being conducted at the Rome Air Development Center. Among the topics considered have been temporal spectra of atmospherically induced phase difference fluctuations, an analysis of an angle-of-arrival apparatus used at RADC and a study of the Fourier transform image restoration procedure. Previous work is summarized, and new results are added where applicable.

DD FORM 1 NOV 65 1473

UNCLASSIFIED
Security Classification

14 KEY WORDS	LINK A		LINK B		LINK C	
	ROLE	WT	ROLE	WT	ROLE	WT
Atmospheric imaging Propagation Angle of arrival Phase difference Image restoration						

INVESTIGATION OF LASER PROPAGATION PHENOMENA

S. A. Collins, Jr.
D. D. Duncan

Contractor: The Ohio State University
Contract Number: F30602-72-C-0305
Effective Date of Contract: 1 April 1972
Contract Expiration Date: 30 September 1973
Amount of Contract: $75,000.00
Program Code Number: 1E20

Principal Investigator: Dr. Stuart A. Collins, Jr.
Phone: 614 422-5045

Project Engineer: Edward K. Damon
Phone: 614 422-5953

Contract Engineer: Raymond P. Urtz, Jr.
Phone: 315 330-3145

Approved for public release;
distribution unlimited.

This research was supported by the Defense Advanced Research Projects Agency of the Department of Defense and was monitored by Raymond P. Urtz, Jr. RADC (OCSE), GAFB, NY 13441 under Contract F30602-72-C-0305.

PUBLICATION REVIEW

This technical report has been reviewed and is approved.

Raymond P. Urtz Jr.

RADC Project Engineer

TABLE OF CONTENTS

		Page
I.	INTRODUCTION	1
II.	ANGLE-OF-ARRIVAL APPARATUS	1
III.	PHASE DIFFERENCE TEMPORAL SPECTRA	5
IV.	IMAGE RESTORATION WORK	8
V.	GENERAL	22
VI.	SUMMARY	23
BIBLIOGRAPHY		24

I. INTRODUCTION

This is the final technical report for Contract No. F30602-72-C-0305. The object of the program has been to provide theoretical studies of selected topics associated with light-beam propagation through a turbulent atmosphere. The efforts were in direct support of the programs being conducted at Rome Air Development Center. Among the topics considered have been temporal spectra of atmospherically induced phase difference fluctuations, an analysis of the angle of arrival apparatus at RADC, and a study of the Fourier transform image restoration procedure.

It is the object of the present report to summarize these studies with emphasis being placed on certain portions of the image restoration work which has received the least coverage in past reports. This will now be done, starting with the angle-of-arrival apparatus.

II. ANGLE-OF-ARRIVAL APPARATUS

The angle-of-arrival apparatus is one built for RADC by the Perkin-Elmer Corporation as part of a multi-purpose apparatus. Past descriptions of this part of the Perkin-Elmer package have been semi-quantitative. The object in this description was to obtain a more quantitative understanding of the device.

Angle of arrival measurements are in general useful because they give angular coordinates of objects. One generally denotes by angle of arrival the angles defining the normal to the wavefront of a light wave originating from a point object. If there are no intervening index fluctuations then the wavefront will be a spherical one centered on the object with normals indicating the direction to the object. If there are intervening refractive index fluctuations, then the arriving wavefront may be different from spherical or may be spherical with a different center or radius of curvature, giving a false measurement.

The device senses angle of arrival fluctuations by examining the position of the focused diffraction limited point image. The transverse displacement, δ, is measured and results are interpreted in terms of angle of arrival, α, by the standard relationship $\alpha = \delta/d$ where d is the telescope image distance.

All angle of arrival measurements are limited. Even in the ideal case measurements having better accuracy than the classical angular resolution determined by the input aperture of the optical system, $1.22\ \lambda/D$ for a round aperture, are difficult. If there are no refractive index fluctuations, the object of a stationary point source is a stationary diffraction pattern, the position of the object being

determined by the center of the pattern. If there is a spherical wavefront with center modified by the index fluctuations, then the diffraction pattern will be centered at a different spot, the amount of displacement being proportional to the apparent angular deviation of the object. If there is a non-spherical wavefront, then the standard diffraction limited pattern is broken up, the amount of degradation depending on the aperture diameter compared with the mean transverse size of the atmospheric fluctuations. The device determines the mean spot position and averages over the spot shape.

The angle of arrival apparatus is shown schematically in Fig. 1.

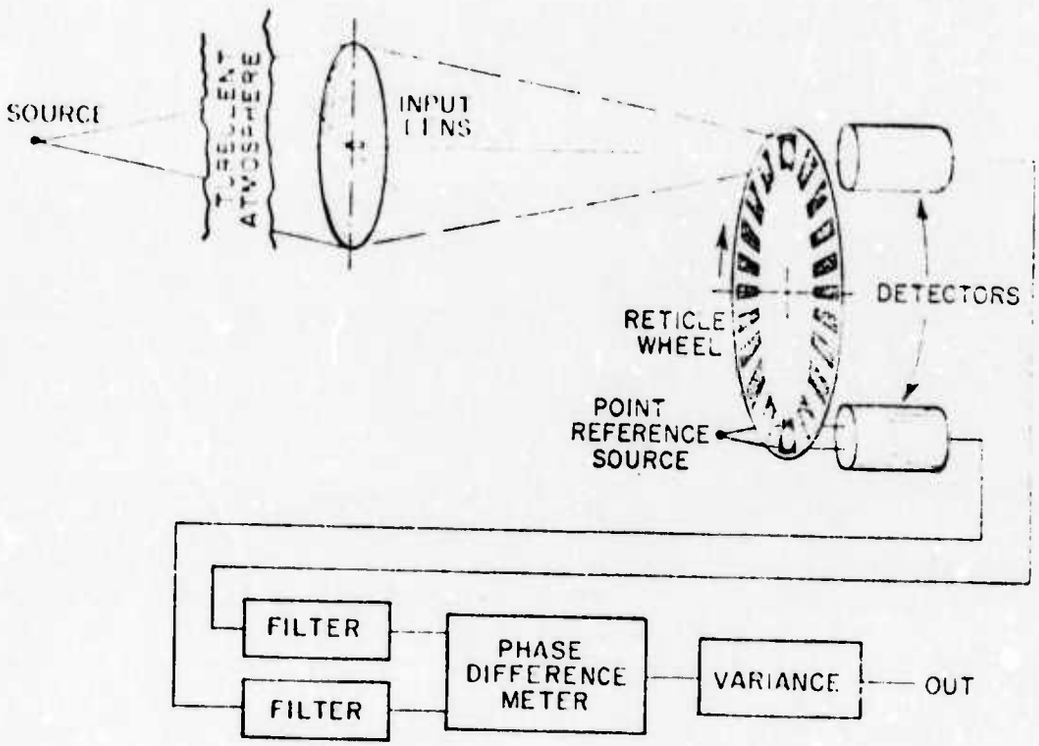

Fig. 1. Angle of arrival apparatus.

Light from a point source degraded by the turbulent atmosphere is collected by the receiving telescope and imaged to a degraded diffraction limited spot. The spot is then chopped with the scanning reticle wheel and applied to a detector. The detector output has the form of a periodic signal, as shown in Fig. 2. The scanning rate of the wheel is sufficiently fast so that the spot is chopped many times before the atmosphere changes it appreciably. The detector output is then filtered

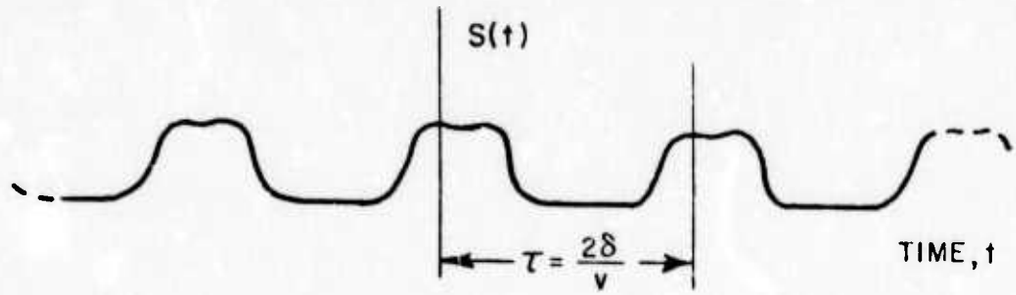

Fig. 2. Typical detector output.

to pass the fundamental frequency. This filtered signal is compared for phase with a standard signal derived from the opposite side of the same scanning wheel. The phase difference is normalized to zero mean, squared and averaged. The mean square phase is then related in the analysis to the angle of arrival variance.

The results of the analysis are presented in terms of one component, κ_x, of the normal $\bar{\kappa}$ to the plane best fitted to the incoming wavefront. The results are based on the assumptions of a Kolmogorov refractive index spatial spectrum and the assumption of negligible amplitude effects. The expression for the mean square angle of arrival, $\langle \alpha_x^2 \rangle$, which the device measures, is then expressed in the form

$$(1) \qquad \langle \alpha_x^2 \rangle = \frac{\langle \kappa_x^2 \rangle}{|\kappa|^2} = \frac{D_\phi(D/2r_o)}{2k^2(D/2)^2} F(N_o)$$

where

$D_\phi(r) = 6.88(r/r_o)^{5/3}$ = atmospheric wave structure function neglecting inner and outer scale effects

D = receiving telescope aperture diameter

$\lambda = 2\pi/k$ = wavelength of incoming light

$N_o = k\delta D/2d$ = Fresnel number based of the size of the slits in the scanning wheel

δ = width of square wave slits in the scanning wheel

d = image distance of receiving telescope.

Equation (1) is very similar to one given by Hufnagel (Hufnagel, 1963). The difference is the slowly varying correction represented by the function $F(N_0)$ of the non-dimensional parameter N_0. Equation (1) can be derived by non-dimensionalizing the pertinent integrals. The function $F(N_0)$ is obtained from the evaluation of a six-dimensional computer evaluated integral. It is shown in Fig. 3. For the RADC

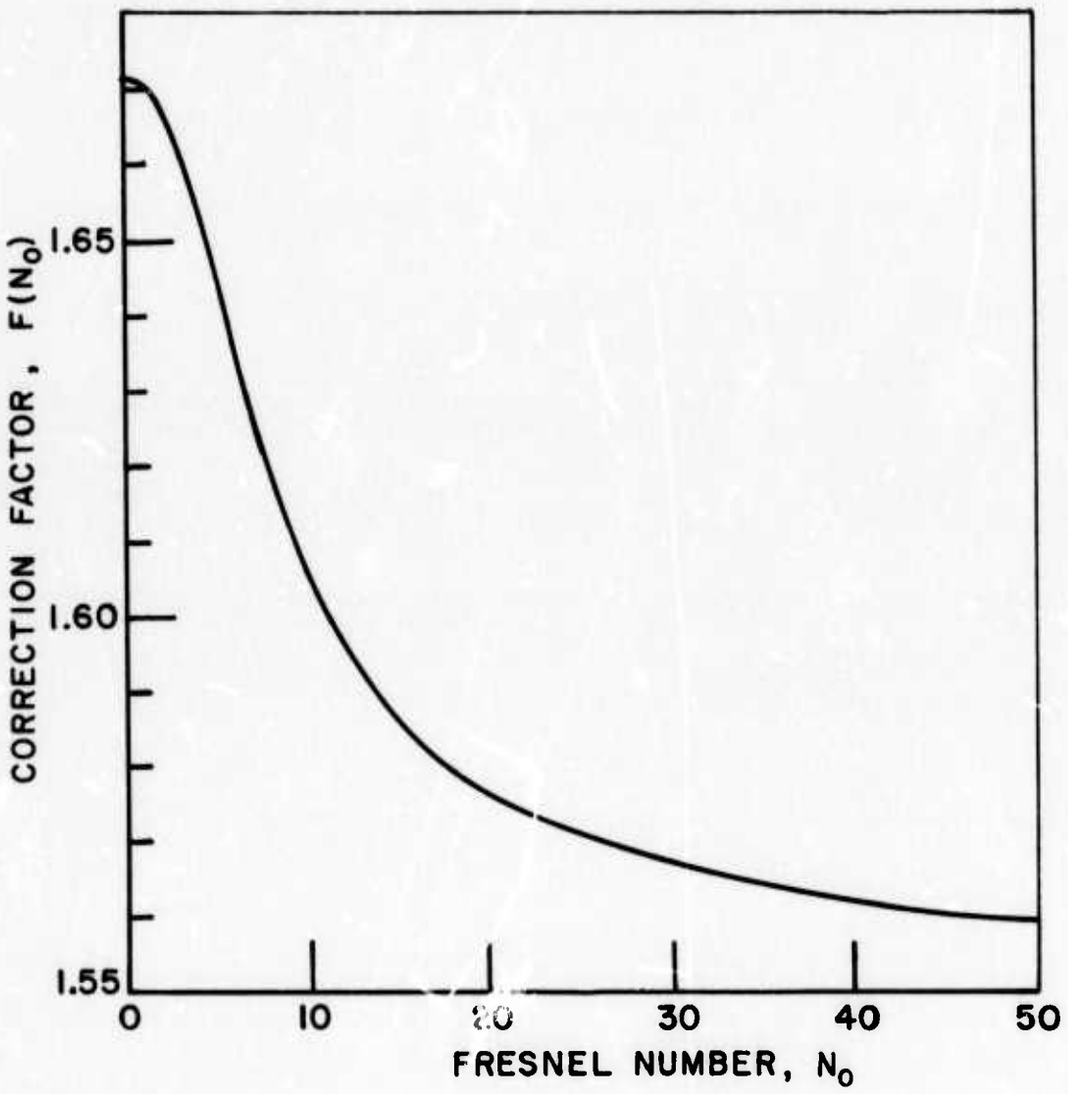

Fig. 3. Correction factor $F(N_0)$.

telescope and apparatus, δ = 2.8 mm, D = 40 cm and 10.6 micron radiation N_0 = 46. so $F(N_0)$ = 1.56.

Equation (1) is the first result. Other pertinent points covered previously (Collins, 1972) are

1) The device does not measure what has been commonly defined as angle of arrival, but does measure something with similar aperture symmetry properties.

2) For very large and very small apertures, arrival angle variance is independent of $N_0 = k\delta D/2d$ (δ = scanning wheel slot size, d = image distance).

3) Only light entering the aperture in a ring of width $d\lambda/\delta$ at the aperture edge is effective in determining the arrival angle variance.

III. PHASE DIFFERENCE TEMPORAL SPECTRA

The second area of investigation was phase difference temporal spectra. The work on temporal spectra is of interest because it provides information on time scales of phase and arrival angle useful to systems designers, and further because phase difference fluctuations are intimately related to angle of arrival fluctuations for small apertures (Zintsmaster, 1971).

More generally, temporal spectral measurements provide a simple method for manipulating experimental data to give a check on our knowledge of the light-beam-turbulence interaction. It is much easier to instrument time-spectral measurements because data need be taken for only one apparatus setting. The corresponding spatial correlations or spatial spectra require many measurements, each with the apparatus adjusted for a different separation.

Temporal correlations and spectra are in themselves useful quantities to compare with theoretical estimates to gain information about atmospheric-turbulence parameters. In this context, they do not suffer from aperture limitations, as do spatial measurements, because readily available time lags are large enough to represent spatial separations much larger than those conveniently available. Thus they provide a convenient optical means with which to examine outer-scale effects, which are important in the low temporal frequency region of the phase difference spectrum. Further we will show that the high temporal frequency dependence of the phase difference spectrum is easily related to the small separation dependence of the phase structure function, thus allowing a convenient experimental check of $D_S(\rho)$.

The physical situation considered is shown in Fig. 4, where a

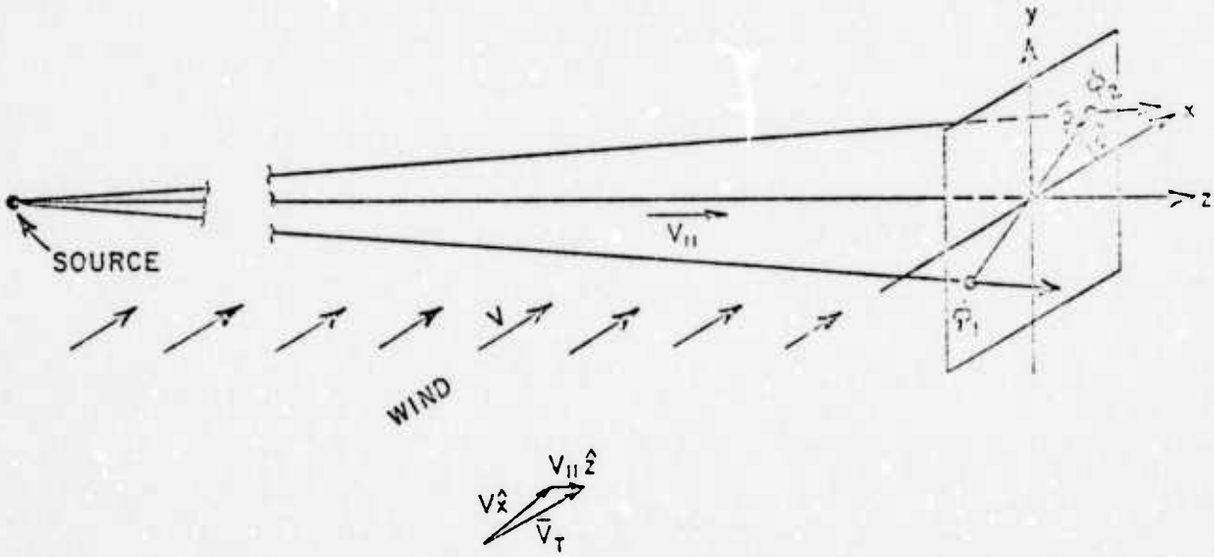

Fig. 4. Diagram of the phase difference spectra situation.

wind of constant velocity $\bar{V}_T$ is blowing. The spherically diverging beam is centered on the z axis. The +x direction is defined so that $\bar{V}_T = V\,\hat{x} + V_{\parallel}\,\hat{z}$, where V is the magnitude of the transverse wind and $V_{\parallel}$ is the component of the wind parallel to the propagation path. $V_{\parallel}$ may be either a positive or a negative quantity. The phase difference $(\phi 2 - \phi 1)$ of two phase points separated by a distance $\bar{\rho}$ in an x-y plane is recorded as a function of time. The vector distance $\bar{\rho}$ makes an arbitrary angle θ with the +x axis, thus enabling us to determine the phase difference spectrum for all relative orientations between the phase points and the transverse component of the wind $(V\hat{x})$. Not shown is that the optical axis specifying the direction of the light beam may be either vertical or horizontal.

Typical results for a horizontal path are presented in Fig. 5 where we see the power spectral density normalized to $8.77k^2LC_n^2\rho^{5/3}$ versus Ω, frequency normalized to $2\pi\rho/V$

where $\lambda = 2\pi/k$ = light wavelength
L = range
C_n^2 = refractive index structure constant
ρ = receiver point separation
V = wind velocity.

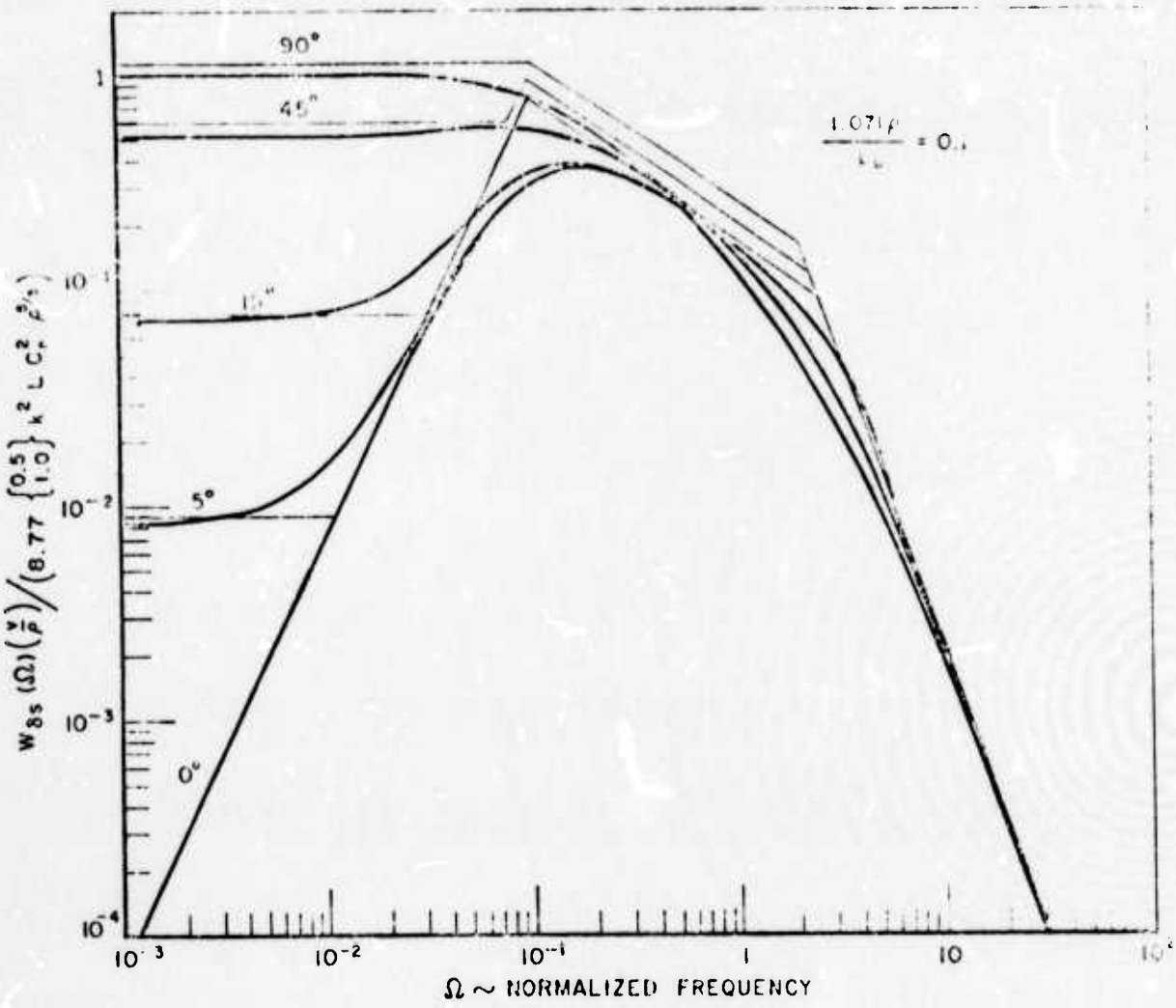

Fig. 5. Normalized phase difference spectrum for a horizontal path versus normalized frequency and orientation angle, when the normalized separation is 0.1.

A "Von Karmann" index spatial spectrum,

$$\Phi(\bar{\kappa}) = .033\left(\left(\frac{1.077}{K_0}\right)^2 + \kappa^2\right)^{-11/6},$$

was chosen so as to include effects of the outer scale, L_0. The more general case where the exponent (-11/6) was replaced by an arbitrary power, ν, was also considered.

Figure 5 shows the general form of the frequency spectrum to be expected for constant horizontal wind velocity, various angles of tilt of the observation points, and point separation $0.1L_o$. Also shown are lines giving asymptotic expressions extracted from the mathematical expressions.

In many situations the wind will have vertical components necessitating an averaging over angle and washing out of detailed angular differences shown in Fig. 5.

In the case of slant paths C_n^2 is proportional to height to the (-4/3) power. The previous spectrum then is multiplied by an additional factor depending on the function h of the maximum and minimum heights, H_{max} and H_{min},

$$h = (H_{max} - H_{min})/H_{min}. \tag{2}$$

The additional factor is graphed in Fig. 6 as a function of h for various relative frequencies. The case considered is a downward slant path. The upward slant path case was considered also and gives different results (Collins, 1972).

This work was prematurely terminated to allow for the study of atmospheric image restoration to be considered in the next section.

IV. IMAGE RESTORATION WORK

The final area of investigation to be considered is a theoretical examination of the Fourier transform method of restoration of atmospherically degraded images. The incentive for this work came from the need to provide information for a proposed series of experiments on the usefulness of the Fourier transform restoration procedure for restoring satellite images using an airplane-born reference source. The work described answered the question whether a collimated beam would be better than a point source on an aircraft flying at a much lower altitude than the satellite. The formalism is also useful in predicting the isoplanatic patch size for this restoration scheme.

The Fourier transform restoration procedure is well known (Harris, 1966). There, one images simultaneously a turbulence degraded object and a turbulence degraded point reference source. If every point in the object and the point reference source are degraded exactly the same, then the quotient of the degraded object spatial spectrum and the reference point spatial spectrum is the restored image spatial spectrum. This is the ideal case. The investigation reported herein considers the situation where the reference source is different

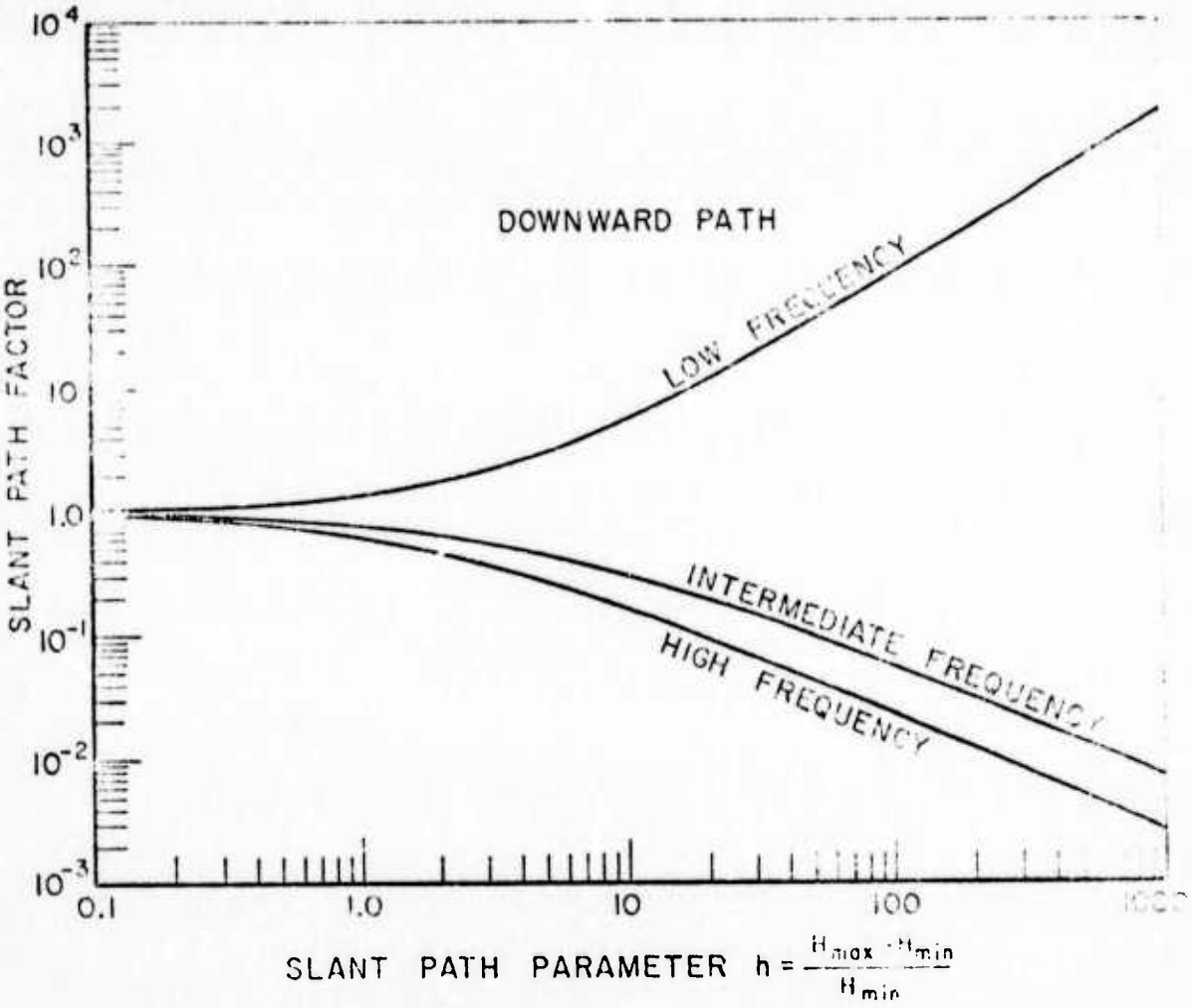

Fig. 6. The additional factor for downward slant path phase difference spectra.

in location from the object so that its image has slightly different degradation from that of the object.

The situation of interest is shown in Fig. 7. We consider two point sources, possibly at different distances from an imaging telescope. The light from the two sources travels through a turbulent atmosphere and is imaged on two image planes appropriate to their distances. One then records the instantaneous intensity patterns and uses them with the appropriate transverse size scaling in the Fourier transform restoration procedure.

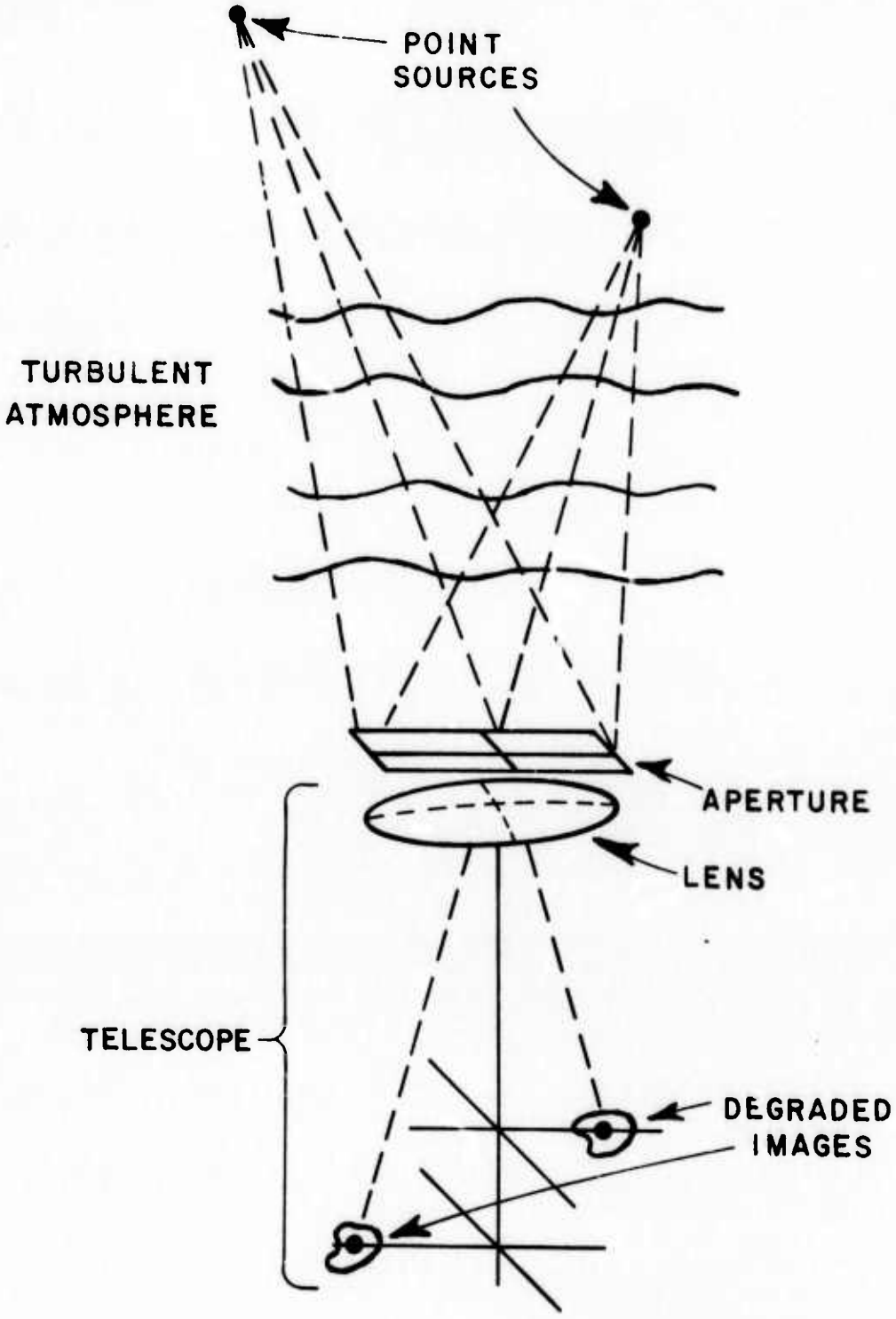

Fig. 7. Schematic illustration of physical situation.

The restoration procedure in this situation is expected to have limitations. The situation becomes complicated if (1) the object points and reference point are not at the same transverse location so that rays from the two partly intersect areas of different index fluctuations, and (2) the object and point reference sources are at different distances from the receiver so that refractive index fluctuations of a given size experience different magnifications by the time they have arrived at the receiver.

One way to overcome the limitation arising when the object is at infinity and the reference source is at a finite distance from the receiver is to use a collimated rather than a point reference source. This would duplicate the point source at infinite distance and should work if the degrading turbulence is between the reference source and the receiver.

The object of these calculations is to assess the effects of displacement of the reference source and to determine the feasibility of using the plane-wave source as a possible remedy in overcoming the effects of longitudinal distance difference.

A model is chosen which allows the mathematics to be greatly simplified. The model is written in terms of the deviations of the turbulence-degraded light wavefront from the undegraded wavefront. These deviations are described mathematically in terms of a series of polynomials in transverse position, $\bar{r}$, which indexes the deviation at any given aperture position. Thus we represent the phase, ϕ, of the light arriving at position $\bar{r}$ in the aperture from a given source in the form

$$\phi(\bar{r}) = \phi_0(\bar{r}) + \phi_1(\bar{r}) \tag{3a}$$

where

$$\phi_1(\bar{r}) = \sum_n a_n F_n(\bar{r}) \tag{3b}$$

and where ϕ_0 represents the phase in the ideal (non-turbulent) case and $\phi_1(\bar{r})$ represents the atmospherically induced fluctuations. The polynomial series similar to that used by Fried (Fried, 1966) are given in Eqs. (4), up through second order.

$$F_1 = \frac{1}{a} \tag{4a}$$

$$F_2 = \frac{\sqrt{3}}{a} \frac{x}{a/2} \tag{4b}$$

(4c) $$F_3 = \frac{3}{a}\frac{y}{a/2}$$

(4d) $$F_4 = \frac{1}{a}\frac{3}{2}\sqrt{\frac{5}{2}}\,(x^2+y^2 - (a^2/6))/(a/2)^2$$

(4e) $$F_5 = \frac{1}{a}\frac{3}{2}\sqrt{\frac{5}{2}}\,(x^2-y^2)/(a/2)^2$$

(4f) $$F_6 = (3/a)(xy)/(a/2)^2.$$

These polynomials are chosen so as to be orthonormal over a square aperture of side "a". It is assumed that the major effect of the atmosphere is represented by the first six polynomials, an assumption born out (at least in the mean square sense) by our calculations and by Fried.

The approach to the problem has two parts describing restoration procedure and the atmospheric interaction, both of which can be stated in terms of the quantitites in Eqs. (3). In the first or restoration part, the Fourier transform restoration procedure is carried out using a particular model for the object and reference input field wavefronts. In the model the wavefronts are deterministic and are represented by one or two terms in the series in Eq. (3b). Indeed for the case considered later, one polynomial (the same one) is used for both the object and reference beam phases. The two wavefronts differ in the size of the coefficients a_n and a_n' multiplying the polynomials; i.e., they have the same shaped wavefront deviation but one is more bent than the other. The quality of the restoration is then investigated as a function of the difference between the coefficients. This allows a limit to be set on the size of the coefficient difference before the restoration procedure breaks down.

In the second, or atmospheric part of the study, the coefficient difference is further related to the atmospheric parameters. Specifically, the root-mean-square coefficient difference is calculated as a function of object-to-reference source separation, range, wavelength, turbulence strength, and receiving plane aperture size, etc. The combination of the image processing and atmospheric calculations for the coefficient difference then allows one to calculate a measure of restoration success for a given set of atmospheric parameters.

The restoration and atmospheric portions will now be outlined and results given.

In the restoration portion of the studies the correlation functions of the object and reference fields were obtained. These then represent

the associated image spatial spectra and the quotient of the two spatial spectra represents the restored image spectrum from which the restored image was obtained. The restored image was then examined using three measures of image quality: the restored image strehl ratio, the integral scale width, and the mean-square difference from the ideal image. The whole process was performed for a series of increasing differences between the object and reference wavefront polynomial coefficients.

Typical results of such a series of calculations are shown in Fig. 8. There we see the normalized integral scale width as a function of coefficient difference for a spherical distortion of 0.75 wavelengths maximum deviation of the object wavefront. We see that the normalized restored image width is unity for zero difference between the wavefronts and initially decreases with wavefront difference. There are further extremely large values, both positive and negative. The large values come from dividing by very small numbers when the spatial spectrum quotient was obtained in the restoration procedure. This process gives rise to unnaturally large values in the restored image spectrum. When the large values cancel there is reasonable restoration. When they do not cancel the restoration procedure fails, as indicated by the very large or very small integral scale width values.

One conclusion drawn from these calculations is that the restoration procedure is reliably valid only within a very small range of differences between the object and reference wavefronts. For larger wavefront differences, either further image processing must be used to prevent the unnaturally large values of the restored image spectrum or a probabilistic description must be used.

The second, or atmospheric part of the study was then aimed at calculating the root-mean-square wavefront deviation arising as a function of atmospheric and other physical parameters. This is then to be compared with the deviation allowed on the basis of the restoration procedure. The complete description of atmospheric effects is quite lengthy, so only the pertinent steps will be documented.

Referring to Fig. 7 for the physical situation, we start by denoting by $(\bar{r},\bar{r}_1)$ the wavefront arriving at $\bar{r}$ in the aperture originating from an object at $\bar{r}_1$, and by a_n its wavefront expansion coefficient. Then using the orthonormality of the functions $F_n(\bar{r})$ in conjunction with Eq. (4b) we have

$$a_n = \int d\bar{r}\, F_n(\bar{r})\phi(\bar{r})W(\bar{r}) \tag{5}$$

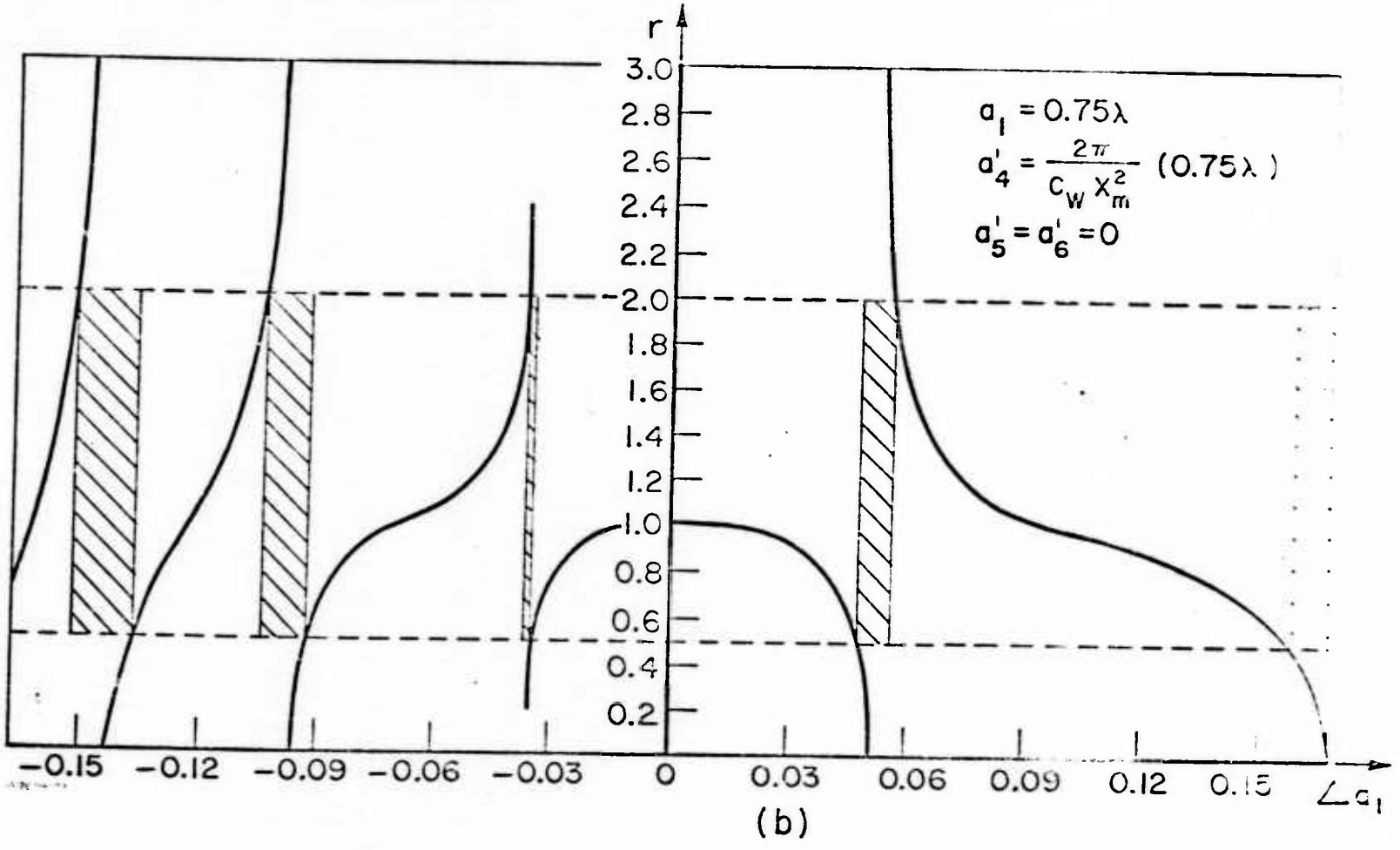

Fig. 8. Graph of normalized restored image integral scale width versus wavefront difference for object wavefront deviation of three quarters of a wavelength.

where $$W(\bar{r}) = \begin{cases} 1 & -a/2 \le x \le a/2, \quad -a/2 \le y \le a/2 \\ 0 & \text{otherwise} \end{cases} .$$

Similarly, denote the wavefront from the source at $\bar{r}_1 + \bar{\rho}$ by $\phi(\bar{r},\bar{r}_1,+\bar{\rho})$, and denote its wavefront expansion by a_n' given by an expression similar to Eq. (5) but with $\bar{r}_1$ replaced by $\bar{r}_1 + \bar{\rho}$. If the two sources are superimposed, then $\bar{\rho} = 0$ and $a_n = a_n'$. For finite values of $\bar{\rho}$, a_n and a_n' are different and a measure of their difference is

$$D_{an}(\bar{\rho}) = \langle a_n - a_n' \rangle^2 , \tag{6}$$

where the brackets indicate ensemble average. From Eq. (5) we have

$$D_{an}(\bar{\rho}) = \left\langle \left| \iint (\phi_1(\bar{r},\bar{r}_1) - \phi_1(\bar{r},\bar{r}_1+\bar{\rho}))F_n(\bar{r})W(\bar{r})d\bar{r} \right|^2 \right\rangle \tag{7a}$$

$$= \iint d\bar{r}\, d\bar{r}'\, F_n(\bar{r})F_n(\bar{r}')W(\bar{r})W(\bar{r}')D_\phi(\bar{r},\bar{r}',\bar{\rho}) \tag{7b}$$

where

$$D_\phi(\bar{r},\bar{r}',\bar{\rho}) = \langle (\phi_1(\bar{r},\bar{r}_1+\bar{\rho}) - \phi_1(\bar{r},\bar{r}_1))(\phi_1(\bar{r}',\bar{r}_1+\bar{\rho}) - \phi(\bar{r}',\bar{r}_1)) \rangle . \tag{7c}$$

The atmospheric effects are introduced in the expression for the phase

$$\phi(\bar{r},\bar{r}_1+\bar{\rho}) = k \int_0^L n(\bar{r}_3)dz_3 \tag{8}$$

and in the expression for the index structure function

$$D_n(\bar{r}_i - \bar{r}_j) = \langle (n(\bar{r}_i) - n(\bar{r}_j))^2 \rangle = C_n^2\left(\tfrac{1}{2}(\bar{r}_i + \bar{r}_j)\right)\left|\bar{r}_i - \bar{r}_j\right|^{2/3} . \tag{9}$$

Using Eqs. (7), (8), and (9), the expression for $D_\phi(\bar{r},\bar{r}'+\bar{\rho})$ simplifies to

$$(10) \qquad D_\phi(\bar{r},\bar{r}+\bar{\rho}) = \frac{k^2}{2}\int_0^L\int_0^L dz_1 dz_2 C_n^2\left(\tfrac{1}{2}(z_1+z_2)\right) \times$$

$$\times\left\{\left|\bar{r}_5-\bar{r}_4\right|^{2/3}+\left|\bar{r}_3-\bar{r}_6\right|^{2/3}-\left|\bar{r}_3-\bar{r}_4\right|^{2/3}-\left|\bar{r}_5-\bar{r}_6\right|^{2/3}\right\}$$

where $\bar{r}_3\cdots\bar{r}_6$ represent points along four rays connecting two aperture plane points to the two source points.

A general expression for $D_\phi(\bar{r},\bar{r}'\bar{\rho})$ can be derived in quite a straightforward fashion. It involves writing the equations for the four lines connecting points $\bar{r}$ and $\bar{r}'$ in the aperture plane with source points at $\bar{r}_1$ and $\bar{r}_1+\bar{\rho}$, (points $\bar{r}_3\cdots\bar{r}_6$ respectively are on these lines) and then substituting in terms of sum and difference coordinates

$$(11a) \qquad \delta = z_2-z_1$$

$$(11b) \qquad \sigma = (z_2+z_1)/2$$

$$(11c) \qquad \bar{\xi} = \bar{r}-\bar{r}'$$

$$(11d) \qquad \bar{\eta} = (\bar{r}+\bar{r}')/2.$$

The final general expression is included here.

$$(12a)\ D_\phi(\bar{r},\bar{r}',\bar{\rho}) =$$

$$(k^2/2)\int_0^{L_1} d\sigma\int_{-\infty}^{\infty} d\delta C_n^2(\sigma)\left\{\left|\bar{r}_5-\bar{r}_4\right|^{2/3}+\left|\bar{r}_3-\bar{r}_6\right|^{2/3}-\left|\bar{r}_3-\bar{r}_4\right|^{2/3}-\left|\bar{r}_5-\bar{r}_6\right|^{2/3}\right\}$$

where

(12b) $$\left|\bar{r}_5-\bar{r}_4\right|^{2/3} =$$

$$[(\xi_x-((\rho_1+\eta_x+\tfrac{1}{2}\xi_x)(\sigma-\tfrac{1}{2}\delta)/L_1)-((\rho_2-\eta_x+\tfrac{1}{2}\xi_x)(\sigma+\tfrac{1}{2}\delta)/L_2))^2$$

$$+(\xi_y-((\eta_y+\tfrac{1}{2}\xi_y)(\sigma-\tfrac{1}{2}\delta)/L_1)+((\eta_y-\tfrac{1}{2}\xi_y)(\sigma+\tfrac{1}{2}\delta)/L_2)^2+\delta^2]^{1/3}$$

(12c) $$\left|\bar{r}_3-\bar{r}_6\right|^{2/3} =$$

$$[(\xi_x+((\rho_2-\eta_x-\tfrac{1}{2}\xi_x)(\sigma-\tfrac{1}{2}\delta)/L_2)-(-\rho_1-\eta_x+\tfrac{1}{2}\xi_x)(\sigma+\tfrac{1}{2}\delta)/L_1))^2$$

$$+(\xi_y-((\eta_y+\tfrac{1}{2}\xi_y)(\sigma-\tfrac{1}{2}\delta)/L_2)+((\eta_y-\tfrac{1}{2}\xi_y)(\sigma+\tfrac{1}{2}\delta)/L_1))^2+\delta^2]^{1/3}$$

(12d) $$\left|\bar{r}_3-\bar{r}_4\right|^{2/3} =$$

$$[(\xi_x+((\rho_2-\eta_x-\tfrac{1}{2}\xi_x)(\sigma-\tfrac{1}{2}\delta)/L_2)-((\rho_2-\eta_x+\tfrac{1}{2}\xi_x)(\sigma+\tfrac{1}{2}\delta)/L_2))^2$$

$$+(\xi_y-((\eta_y+\tfrac{1}{2}\xi_y)(\sigma-\tfrac{1}{2}\delta)/L_2)+((\eta_y-\tfrac{1}{2}\xi_y)(\sigma+\tfrac{1}{2}\delta)/L_2))^2+\delta^2]^{1/3}$$

(12e) $$\left|\bar{r}_5-\bar{r}_6\right|^{2/3} =$$

$$[(\xi_x+((-\rho_1-\eta_x-\tfrac{1}{2}\xi_x)(\sigma-\tfrac{1}{2}\delta)/L_1)-((-\rho_1-\eta_x+\tfrac{1}{2}\xi_x)(\sigma+\tfrac{1}{2}\delta)/L_1))^2$$

$$+(\xi_y-((\eta_y+\tfrac{1}{2}\xi_y)(\sigma-\tfrac{1}{2}\delta)/L_1)+((\eta_y-\tfrac{1}{2}\xi_y)(\sigma+\tfrac{1}{2}\delta)/L_1))^2+\delta^2]^{1/3}.$$

In Eqs. (12) L_2 and L_1 are the distances of the reference source and object respectively and ρ_2 and ρ_1 are respectively the transverse coordinates of the reference source and the object: $\bar{\rho}=\bar{\rho}_1+\bar{\rho}_2$. It has further been assumed that the lateral source displacements are only in the x direction. With the variable transformations in Eqs. (11), Eq. (7b) becomes

(13) $D_{an}(\rho) =$

$$\int d\bar{\xi}\int d\bar{\eta} F_n(\bar{\eta}+\tfrac{1}{2}\bar{\xi})F_n(\bar{\eta}-\tfrac{1}{2}\bar{\xi})W(\bar{\eta}+\tfrac{1}{2}\bar{\xi})W(\bar{\eta}-\tfrac{1}{2}\bar{\xi})D_\phi(\bar{\xi},\bar{\eta},\bar{\rho}).$$

The evaluation of Eqs. (12) and (13) is straightforward but lengthy. It has been performed for three special cases: object and reference both at infinite distance, corresponding to an object at satellite height and collimated reference beam coming from an aircraft; object at infinite distance and reference at finite distance corresponding to object at satellite height and point reference on an aircraft; and object and reference both at finite distance, corresponding to using a point reference on an aircraft to restore the image of another aircraft at the same height. The expressions have also been evaluated for the situation where the refractive index fluctuations are confined to one very thin "delta function" layer at a given height, and where the source and reference are at the same and different heights. The integrals were evaluated numerically.

Typical results are shown in Fig. 9. There we see the RMS wavelength difference corresponding to coefficient a_4 graphed as a function of ρ for point sources at 20 km and 150 miles and point reference at 20 km. Further two turbulence conditions were considered. The two bottom curves show the effects of surface level turbulence

$$(C_n^2(z) = (z/z_o)^{-4/3})$$

for the two different objects and the two top curves show the effects of a high altitude turbulence layer at 17 km altitude. These curves apply specifically for coefficient a_4 which implies only a spherical deformation of both object and reference beams. Similar curves for coefficients a_5 and a_6 with hyperbolic wavefront centered on the axis and aperture diagonals are shown in Figs. 10 and 11 respectively.

The strength of the high altitude turbulent layer was chosen so as to provide the same values for a plane wave wave-structure function at the ground for a point source at infinite range and turbulent layer,

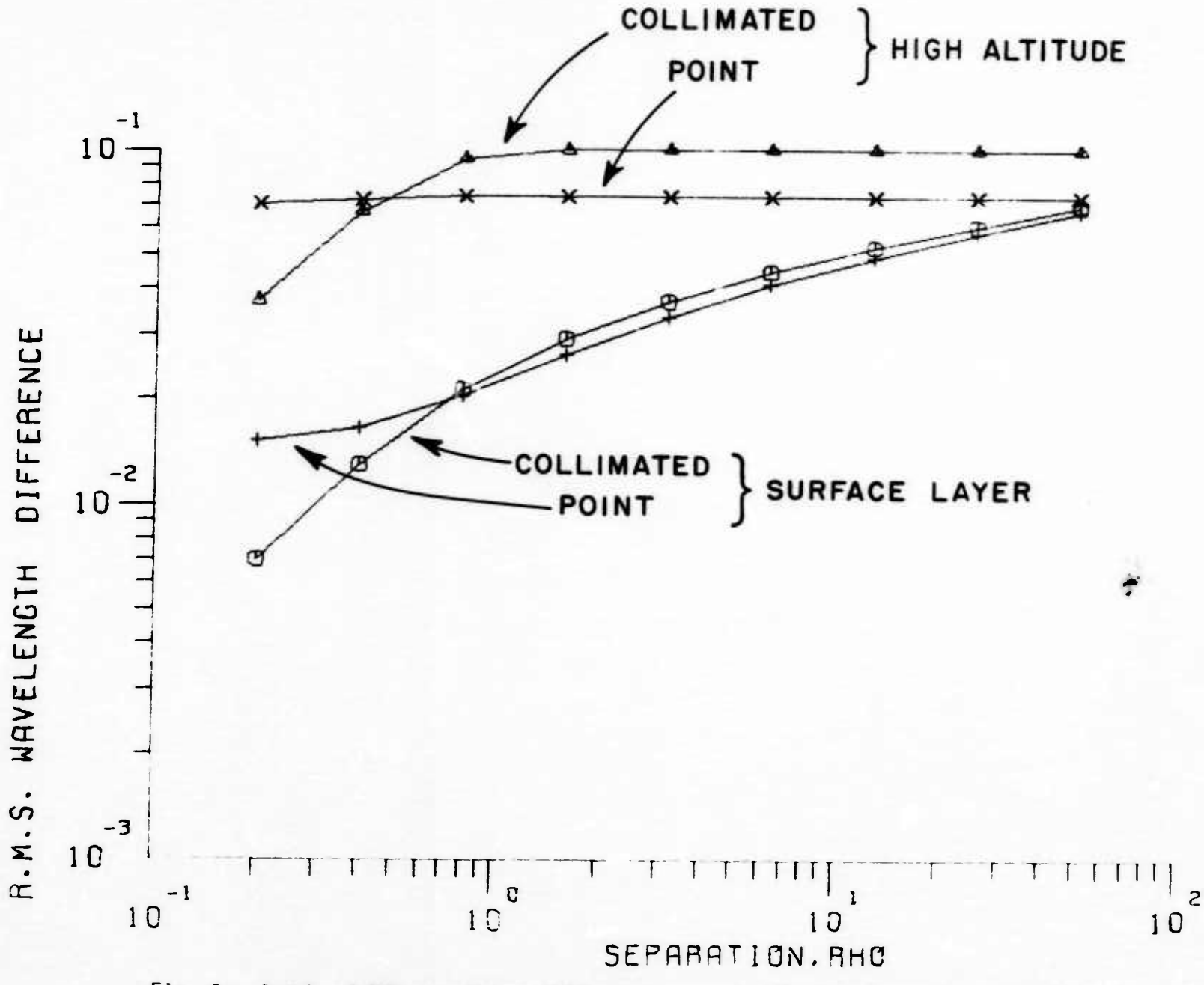

Fig. 9. Graph of RMS wavefront difference versus object-reference source distance.

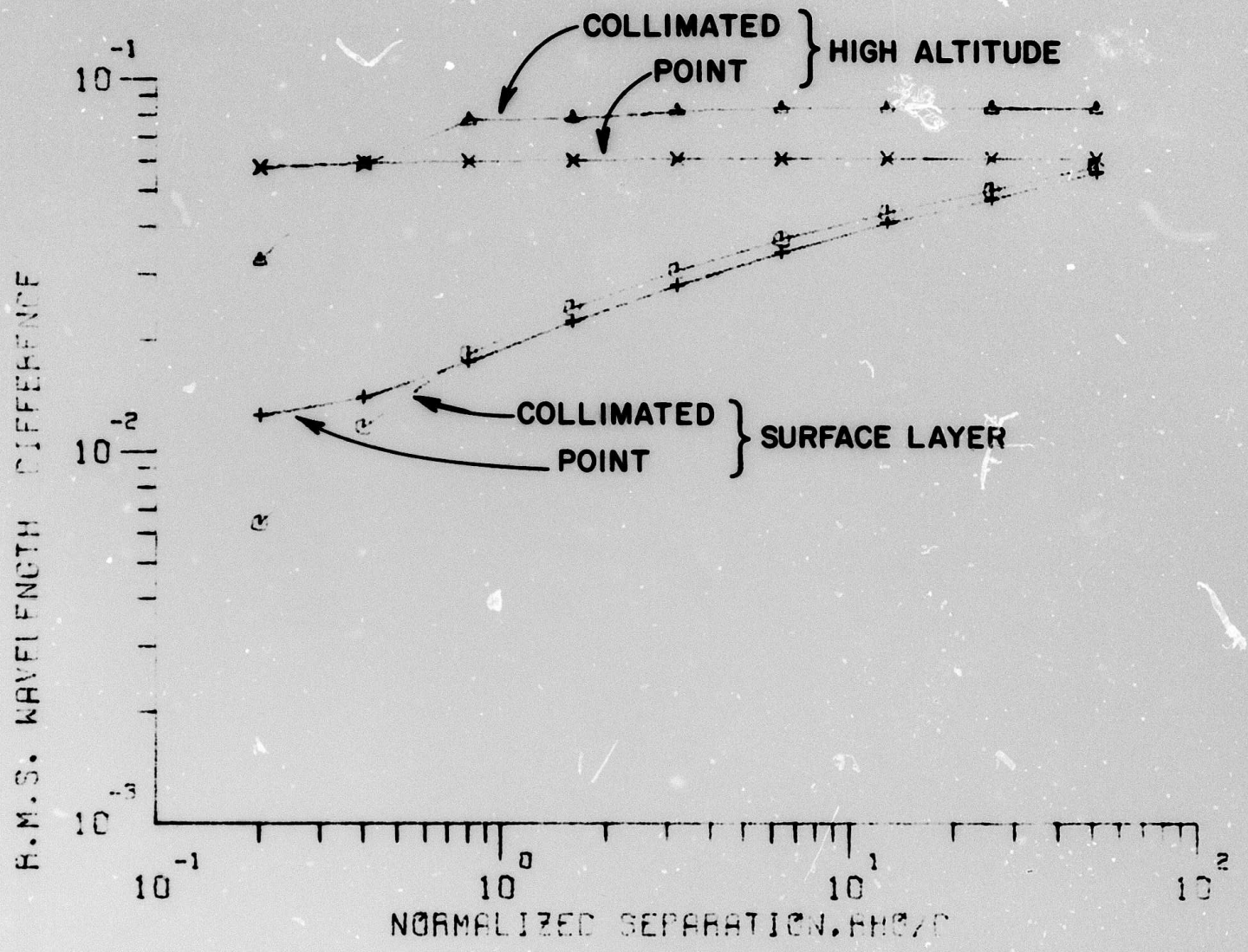

Fig. 10. Graph of RMS wavefront difference versus object-reference source distance; coefficient a_5.

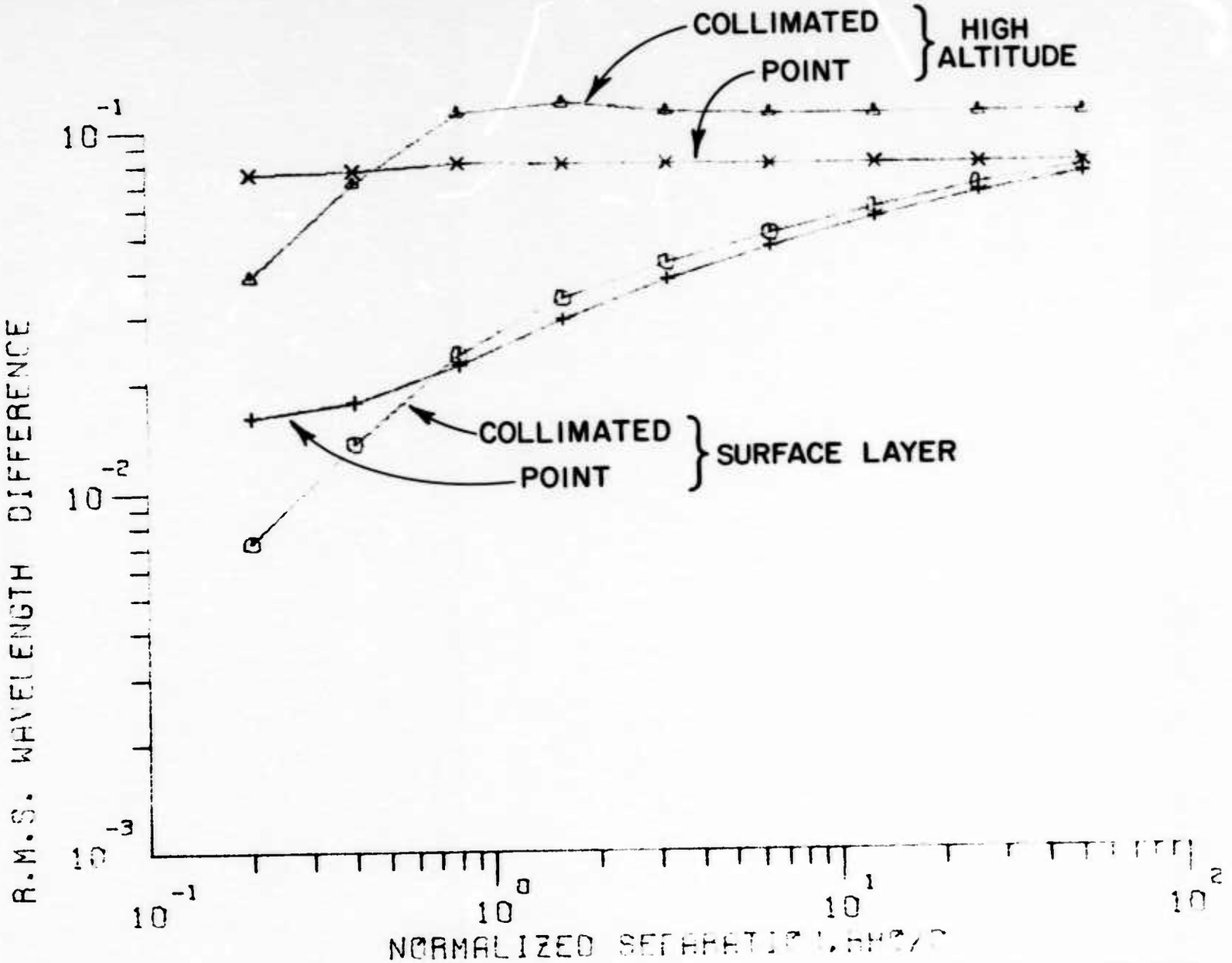

Fig. 11. Graph of RMS wavefront difference versus object-reference source distance; coefficient a_6.

as due to ground level turbulence, and point source at infinity. The calculations were made for $\lambda = 0.5\mu$ and $C_n^2 = 2.1 \times 10^{-16}$ at one meter height.

The curves exhibit some expected behavior. For the cases where point object and reference are both at 20 km height, the RMS wavefront difference goes to zero as ρ becomes small. This is expected since light from both (point) sources ends up traversing regions of the same refractive index fluctuations. For the case where one source is at a different height than the other, there is a residual value for the RMS wavefront difference even when $\rho = 0$. This is because a given index fluctuation magnifies light differently from sources at different distances, and there is complete cancellation only for very low level turbulent fluctuations. It is also noted that the effect of the high-level turbulent layer is significantly greater than that due to the ground level turbulence. That is, a small separation of rays from the two sources produces a much greater effect in interacting with high level index fluctuations than with ground level fluctuations, due to the wavefront magnification of spherical waves.

The curves can be useful in deciding whether restoration is possible in a given situation. For example, if a value of 0.01 wavelengths difference can be tolerated for the wavefronts then a very close spacing between reference and image must be obtained or there must be weaker turbulence. If a value of 0.10 is acceptable, then, with the value of C_n^2 chosen, a source separation of one aperture size is allowed.

One other point is indicated. That concerns the relative ease of restoration for objects at the same height as the reference, compared with objects much higher than the reference. Figure 3 indicates that for object and reference separated by more than one aperture size, the ease of restoration is almost the same, the values of the RMS wavefront difference lying within a factor of two of each other for $\rho/a \geq 1$.

Further work remains to be done in this area especially on the restoration portion of the effort. That involves investigating the use of a smoothing function in the restored image spectrum to remove the unnatural singularities coming from dividing by small numbers. That will provide more physically meaningful restored images and better numbers on the restored image quality indices with which to compare the mean square wavefront deviations.

V. GENERAL

In addition to the work outlined, the bibliography lists one paper that has been published Reinhardt, 1972) and three that are in the preparation stages; (Davidson 1974), (Collins, 1974a), (Collins, 1974b).

VI. SUMMARY

This contract has considered several problems, all aimed at providing support to work being carried out in connection with RADC programs. The problems are phase difference temporal spectra predictions, analysis of the angle of arrival measurement apparatus used at RADC, and theoretical study of the Fourier transform method of restoration of atmospherically degraded optical images. In each case theoretical predictions were completed and where called for recommendations made and conclusions drawn.

BIBLIOGRAPHY

(Hufnagel, 1963), Hufnagel, R.E., "Understanding the Physics of Seeing Through Turbulent Atmospheres," Paper presented at Patrick Air Force Base, Florida, (1963).

(Fried, 1966), Fried, D.L., "Statistics of a Geometric Representation of Wavefront Distortion," J. Opt. Soc. Am., 56, p. 1372, (1966).

(Collins, 1972), Collins, S.A., Jr. and Reinhardt, G.W., "Investigation of Laser Propagation Phenomena, Quarterly Report 3432-3, ElectroScience Laboratory, Department of Electrical Engineering, The Ohio State University; prepared under Contract F30602-72-C-0305 for Rome Air Development Center, Griffiss Air Force Base, New York.

(Collins, 1974a), "Analysis of an Angle of Arrival Measurement Apparatus," to be published.

(Collins, 1974b), Collins, S.A., Jr. and Duncan, D.D., "A Study of Atmospheric Effects in the Fourier Transform Image Restoration Procedure," to be published.

(Davidson, 1974), Davidson, R.S., II and Collins, S.A., Jr., "A Study of Wavefront Differences in the Fourier Transform Method of Image Restoration," to be published

(Harris, 1966), "Image Evaluation and Restoration," J. Opt. Soc. Am., 56, p. 569.

(Reinhardt, 1972), Reinhardt, G.W. and Collins, S.A., Jr., "Outer Scale Effects in Turbulence-Degraded Light Beam Spectra," J. Opt. Soc. Am., 62, p. 1526.

(Zintsmaster, 1971), Zintsmaster, L.R., "Angle of Arrival Calculations at 10.6μ," Report 3163-1, June 1971, ElectroScience Laboratory, Department of Electrical Engineering, The Ohio State University; prepared under Contract F30602-72-C-0305 for Rome Air Development Center, Griffiss Air Force Base, New York.